Integrating Multi-Length Scale High Resolution 3D Imaging and Modelling in the Characterisation and Identification of Mechanical Failure Sites in Electrochemical Dendrites

Moshiel Biton, Farid Tariq, Vladimir Yufit, Zhangwei Chen, and Nigel Brandon

Department of Earth Science and Engineering, Imperial College London, London, UK

Corresponding author: m.biton13@imperial.ac.uk, +447799600354

Abstract

The Zn-air battery system is attractive because of its potentially high power density, environmental compatibility and low-cost materials [1]. This paper is focused on understanding the degradation of Zn air batteries, in particular the evolution of Zn dendrites, one of the main degradation mechanisms. Complementary tomographic techniques allow the direct 3D imaging and characterisation of complex microstructures, including the observation and quantification of dendrite growth. Here we present results from 3D x-ray and FIB-SEM tomography of Zn dendrite formation in a zinc-air battery, down to resolutions of tens of nanometers, enabling analysis of complex micro-structures. This approach is shown to be effective in understanding how electrochemical dendrites grow, and demonstrates that tomography coupled with modelling can provide new insights into dendrite growth in electrochemical systems.

1. Introduction

The Zn-air battery system is attractive because of its high power density, environmental compatibility and low-cost materials.[1],[2] The rechargeable zinc electrode is based on the formation of insoluble ZnO in the electrode on discharge, that is reduced to metallic zinc on charging.

In the Zn-air system, when charging, Zn dendrites may grow out from the anode and possibly penetrate the separator, leading to Zn loss and eventually an internal short-circuit when the dendrites reach and contact the cathode. Dendrite growth is not limited to the Zn systems and is one of the failure mechanisms in various Li-ion battery systems as well.[3]

In order to improve battery performance it is important to characterise real electrode structures and understand how their 3D structure may affect performance.[4] X-ray and dual focused ion beam and scanning electron microscope (FIB-SEM) technology have been attracting interest in the field of batteries and fuel cells to characterise their electrode structure.[4-9]

Yufit *et al* recently presented work showing the application of 3D imaging to monitor the growth of multiple dendrites in the Zn-air system. This work focuses on a novel approach for high resolution 3D imaging of a single dendrite, linking this with mechanical in-situ testing and computational modelling to better understand the nature and properties of dendrites formed in the Zn-air battery system.[20]

2. Experimental

A new methodology was developed to capture high resolution 3D images of a single Zn dendrite. This was achieved by cutting a small piece of carbon tape and attaching a single dendrite onto it under a microscope (Figure 6). The dendrite was then covered with a micro drop of epoxy of a volume of 0.5- 20 μl using a micropipette to ensure its mechanical stability during the Zeiss Auriga FIB-SEM slice and view process (Figure 7). Imaging was carried out using a Ga ion beam of 30 kV with current 20 nA was used to serially section and polish the sample surface while an electron beam captured secondary electron images of the surface. The process was repeated until 300 images were captured to provide a full size dendrite. Image foreshortening and alignment corrections were applied using FEI Avizo Fire 8 and reconstruction of the data.

Prior to modelling, the measured 3D microstructure of the dendrite with the neck connecting to the square base was converted into a volumetric finite-element (FE) mesh using Simpleware ScanIP combined with adaptive meshing strategy (Simpleware, Exeter, UK). After meshing, the model was imported into ABAQUS CAE (Dassault Systèmes, France) for static loading simulation. The base of the model was fixed with no displacement or rotation permitted. One of the branches near the top of the dendrite was statically loaded with a point force parallel to the base plane for the simulation of the bending process performed in accompanying micro-mechanical measurements using micromanipulator, Kleindiek Nanotechnik, (Reutlingen, Germany). The in-situ micro bend test was carried out using the MM3A-EM micromanipulator shown in Figure 10a inside an Auriga 40 FIB-SEM for high resolution imaging simultaneously to the bending test, and is described in detail elsewhere [10, 11]. In this study, a mechanical model of a single dendrite is demonstrated;

the dendrite is considered as polycrystalline zinc, with a Poisson's ratio of 0.26 and an elastic modulus of 97 GPa[12], with the assumption that the polycrystalline zinc is isotropic, linear and elastic. A maximum principal stress criterion was considered in this study to identify the critical stress, and hence, the critical force required to fracture this particular single dendrite.

3D imaging and tomography of the cell was carried out using GE Phoenix v|tome|x and GE Phenix Nanotom S X-ray micro-CT machines (GE, Boston, USA) X-ray. The electrochemical cell was placed into the X-ray machines for in-operando radiography and 3D tomography experiments.

A new generation of a Zn-air cell was designed to study the early stages of the growth. Dendritic growth was established from a polished Zn tip with a diameter of 200 μm.

The cells were modified and only a small area, 0.0314 mm^2, of the Zn tip took part in the reaction. This enables *in-situ* X-ray imaging experiments and to focus only in a small area, in higher resolution and field of view (FOV) than previous experiments. The modification steps that were taken are shown in Figure 1. First the cell was filled with epoxy to cover the Zn tip (Figure 1a), the excess epoxy material above the tip was removed using an Accutom 50 (Struers, Copenhagen, Denmark), and then polished to produce a flat surface with an area of 0.0314 mm^2 and to expose only a small area of the Zn tip.

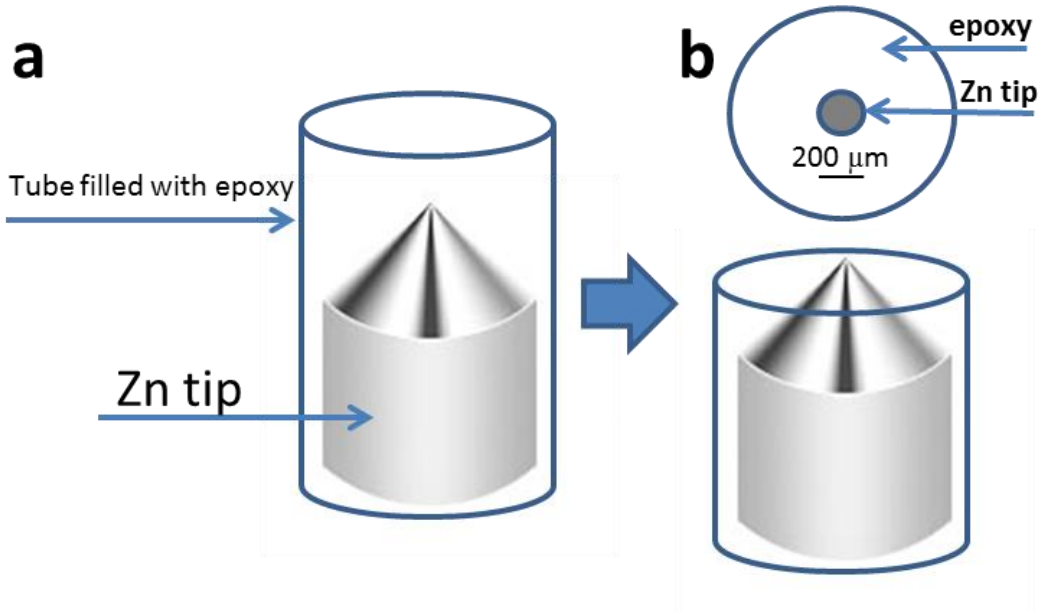


Figure 1 Schematic illustration of the new cell procedure (a) the original cell is filled with epoxy. (b) Cut and polished - on the top, a plan view of an epoxy surrounded Zn tip, with a diameter of 200 μm, is shown.

Since the tip or the active area is much smaller than that of the one in previous experiments (i.e. only a circle with a 100 μm radius compared to the whole tip), 2 mA current was found to be sufficient in order to observe massive dendrite growth, as can be seen in Figure 4i.

3. Results and Discussion

A study of dendrite formation in the Zn-air battery system, which is one of the main degradation mechanisms[13]; was reported previously in this chapter. SEM images (Figure 2) of the Zn tip were taken in order to better understand dendrite microstructure in high resolution.

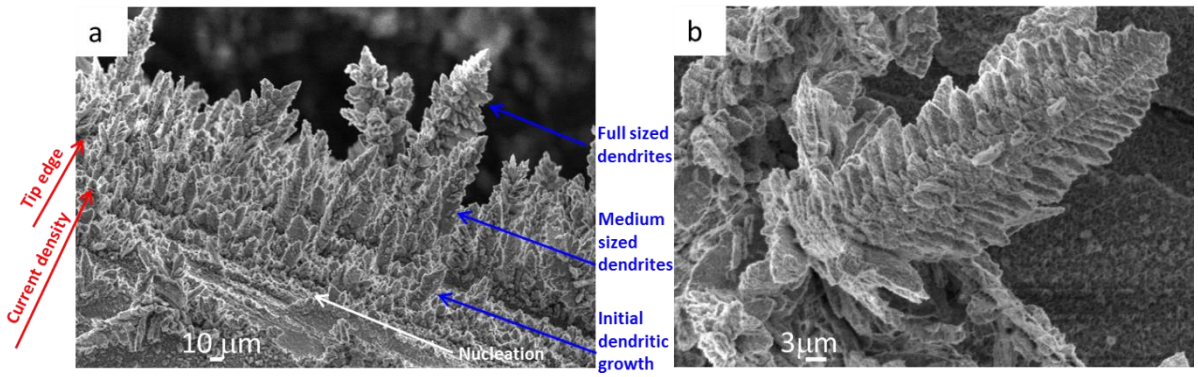


Figure 2 SE SEM images (a) evolution of Zn dendrite on the Zn anode (b) close-up of single dendrite.[14]

The evolution of the dendrites from the nucleation stage through the entire growth to the full sized dendrite can be seen in Figure 2a. At the edge of the tip, full sized dendrites are seen. In that location the current density is higher resulting in the highest observed growth rate. X-ray tomography imaging was then carried out to capture the geometry of the dendrites in 3 dimensions and to provide surface to volume ratio and quantitative insight into the shape, size, roughness and network of the dendrites.

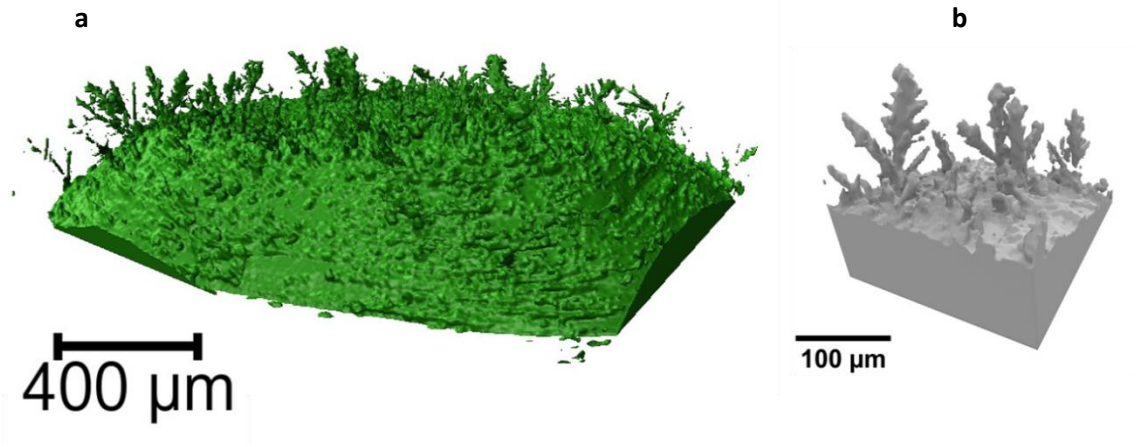


Figure 3 3D rendering of zinc electrode after initial growth (a) tip (b) group of individual dendrites

Long dendrites grow out from the surface of the bulk Zn tip, with competitive growth in denser regions of dendrites (Figure 3). Dendrites' arms grow outwards from the main trunk to form branches, which can also display herringbone type needles growing out of them. As mentioned earlier, the final structure after 15 minutes of charging at 10 mA appears as a dense array of dendrites of various heights, roughly reaching ca.200 µm from the bulk surface.

2 mA current was applied for 15 minutes in order to observe the different steps of the dendritic growth which are presented in the radiographs in Figure 4. It is seen from the radiographs shown in Figure 4 and from the video (supplementary material) that the dendrites are continually growing and do not coalesce.

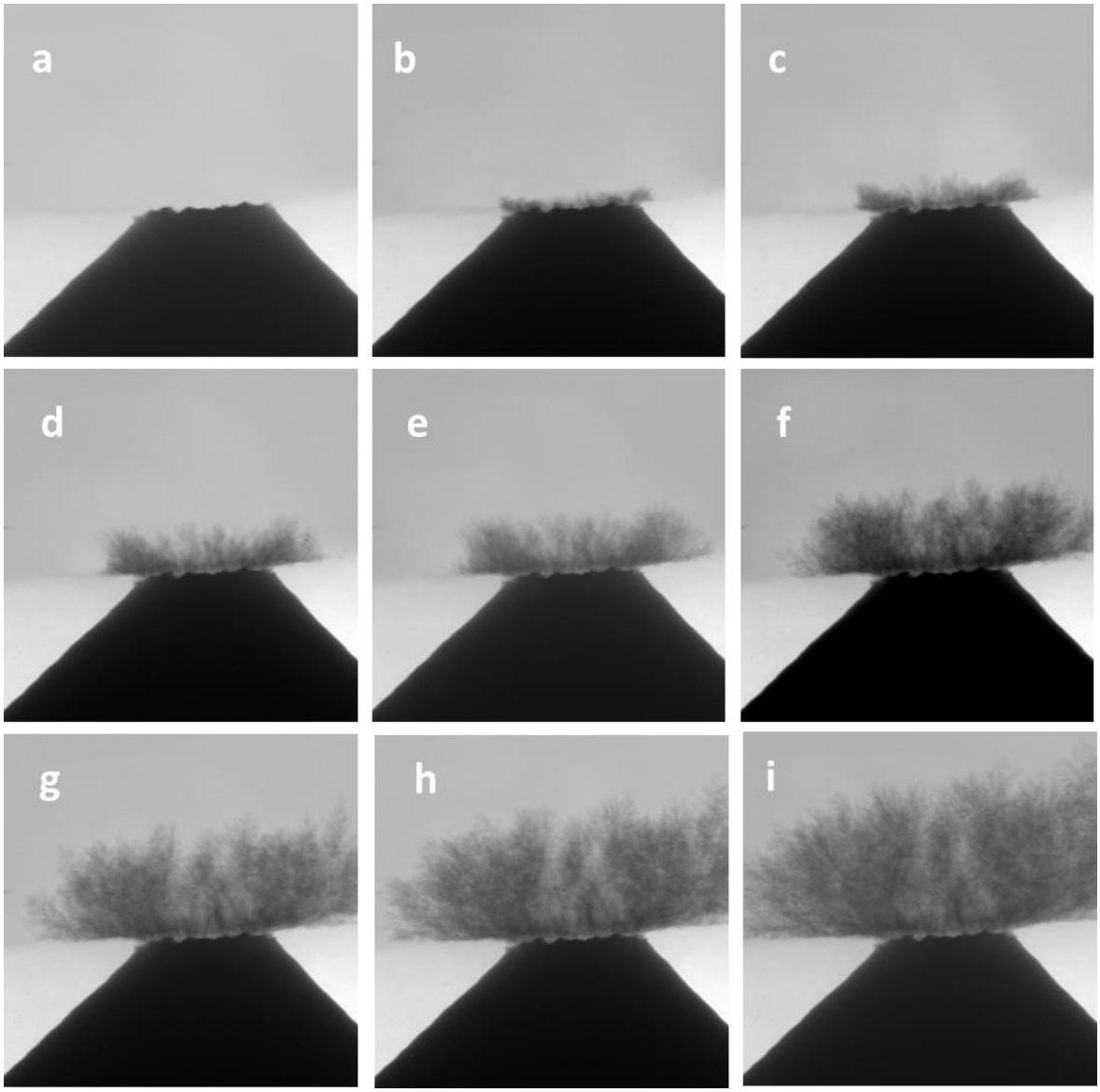


Figure 4 Radiography images of the different stages of the dendritic growth at 2 mA: (a) 0 sec (b) 50 sec (c) 120 sec (d) 200 sec (e) 300 sec (f) 450 sec (g) 600 sec (h) 750 sec and (i) 900 sec.

As indicated, rather than coalescing growing dendrites form a dense "forest" like microstructure with the presence of free hanging and intertwined branches.

Surface roughness, full size dendrite and secondary features cannot be seen in detail using X-ray imaging and tomography (Figure 3 and Figure 4). High resolution (typically <100 nm) is required to accurately capture the dendrite structure, which can be readily achieved using FIB-SEM techniques.

From Figure 5b it is possible to see some branches of a zinc dendrite using lab source X-ray imaging, but not the full size of the dendrite at high resolution as this is too large for the available field of view.

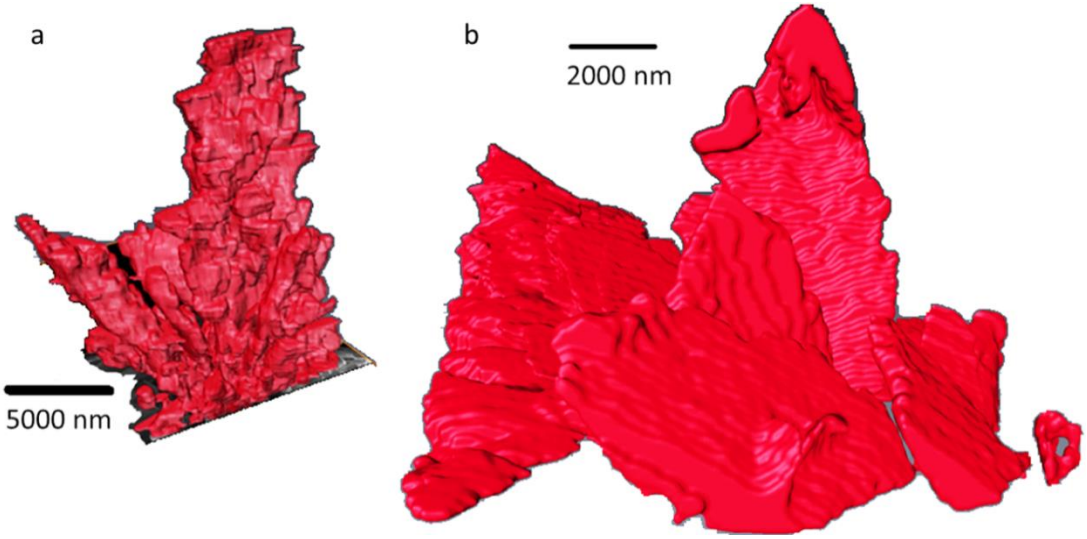


Figure 5 Unsuccessful results of FIB-SEM Tomography images after segmentation and reconstruction (a) without epoxy (b) with epoxy impregnation.

Ex-situ analysis of the dendrite microstructure was carried out using the FIB-SEM technique. The 3D image of the dendrite in Figure a is a result of a dendrite which was milled, imaged, reconstructed and segmented without keeping it in place with epoxy; the resulting 3D structure was mechanically unstable during the slice and view process and misalignment between the slices caused a noisy and low quality image. In Figure b, branches of impregnated epoxy dendrites sample are shown. The epoxy covered the surface and was added to bring mechanical stability to the dendrite branches during the milling process. Achieving high resolution 3D FIB-SEM imaging of a full single dendrite is a difficult task as it is necessary to precisely mill the volume that contains the full dendrite. An example of an unsuccessful process for achieving the desired 3D full dendrite image is presented in Figure 5b, instead of a full dendrite only segmented branches of dendrites are seen. Thus, a new

methodology for imaging a single dendrite (Figure 2b) was developed as described in the Experimental section and presented in Figure 6 and Figure 7.

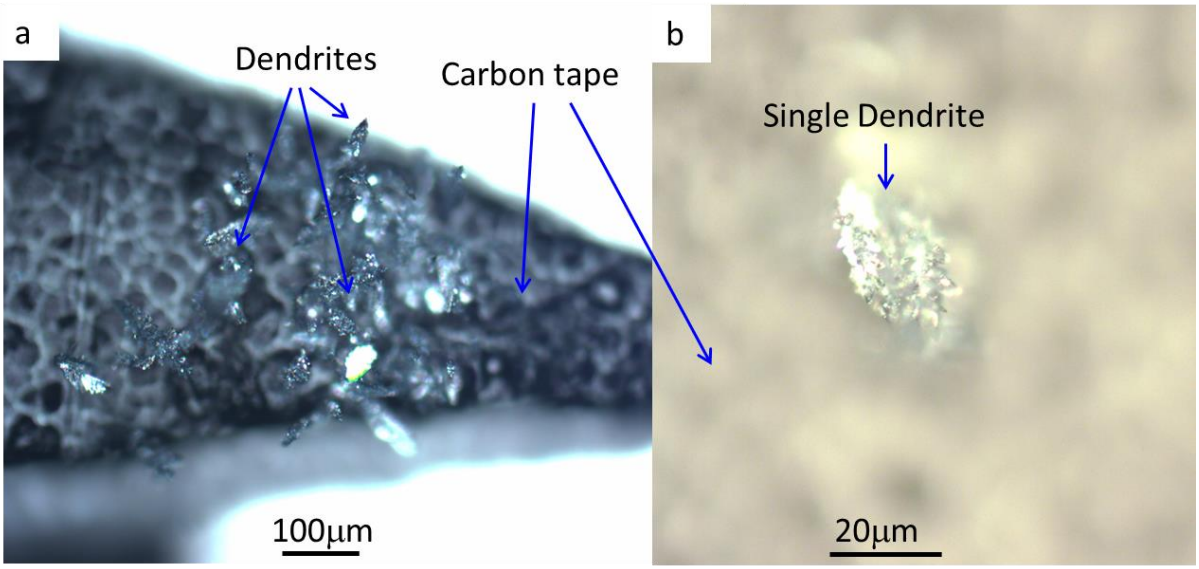


Figure 6 Optical microscope images of dendrites after detaching them from the carbon tape (a) several dendrites and (b) single dendrite.

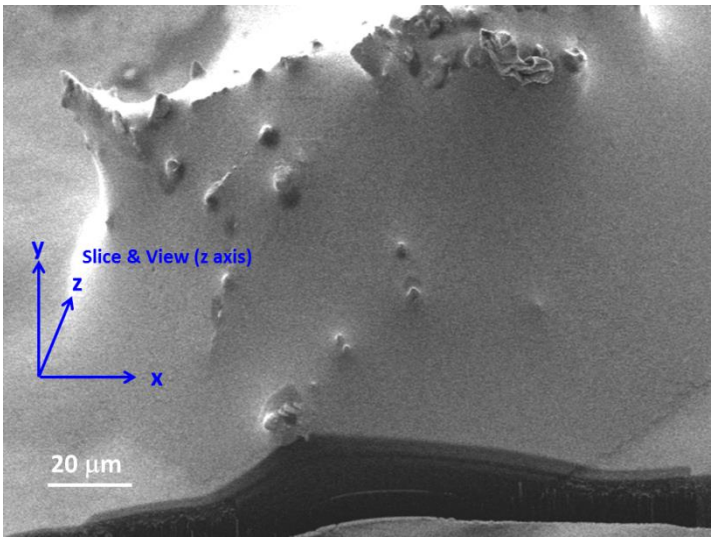


Figure 7 SEM image of a 2D slice in high resolution in the 'slice and view' process, the slicing occurred in the Z direction; a 'micro-drop' of epoxy covered a full dendrite.

The slice and view direction is represented by the blue arrow (Figure 7-Z direction), the micro drop of epoxy was dropped on the area which can be seen in Figure 7.

A high resolution 3D image, with a lateral resolution of 500 nm pixel size, of a full size single dendrite is presented in Figure .

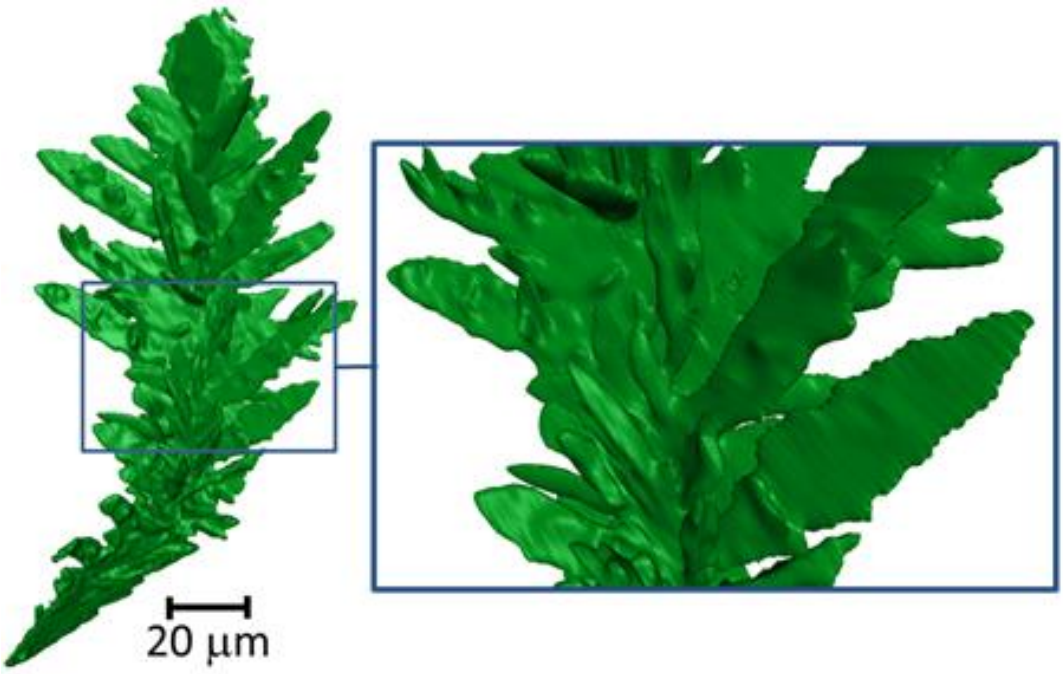


Figure 8 Reconstructed 3D image of a single zinc dendrite obtained using FIB-SEM tomography

The advantage of the FIB-SEM technique in terms of resolution, in addition to the complementary X-ray tomography technique, is clearly seen in Figure . Using the FIB-SEM it is possible to see small features in a 3D image which were not possible to examine using X-rays in this study. However, it is important to note that higher resolution images could still be obtained by X-ray tomography using a synchrotron source. The FIB-SEM data reveals thinner and smaller branches as well as the roughness of the surface of the dendrite along secondary dendrites which cannot be observed in the X-ray image. While the reconstructed dendrite is not the largest dendrite present (c.a. 150 μm) the results show similar characteristics for most of the deposited dendrites. The dendrite stem is not entirely straight and starts to bend at c.a. 60 μm from the bottom, probably as a result of interactions with the surrounding dendrites as they grow, or possibly due to damage arising

from sample preparation. The stem at the bottom (the part that was attached to zinc electrode) is only 5 μm in length with no large branches grown on it up to a height of around 60 μm. In contrast the middle part of the dendrite has branches/secondary dendrites, some of which extend up to 30 μm from the trunk. At the top of the dendrite the length of the branches decreases to c.a. 10 μm. It is possible to discern nucleation sites on the arms where ternary branches could start to grow.

Skeletonised visualization (carried out using Avizo software) of the dendrite presented in Figure is shown in Figurea describes a network of the dendrite branches and how they are connected; quantification (10b and d) confirms that there are more neighbours in the dense region, a region which contain more branches and secondary and ternary dendrites. Each coordination number (which refers to the integer of connections between the neighbouring nodes) as a function of distance from the anode is represented as a separate box (Figureb). Box-and-whisker plots were introduced by the statistician Tukey in 1977 for the purpose of giving rapid visualization of data [15]. These displays have been found to be useful in numerous areas. It has found that such displays can be effectively used for the presentation of the coordination number as a function of distance from the anode. The box is determined by the 25th and 75th percentiles of coordination number population as distance from the anode while the whiskers are determined by the 5th and 95th percentiles (See Figurec). Additional values including the minimum, median (the line inside the box), mean (the small square inside the box), the 1st (the small X on the edge at the bottom) and 5th (the horizontal line on the edges at the bottom) percentiles, and 95th and 99th (same as at the bottom on the opposite edge) percentiles are presented (Figurec explains how to read the data in Figureb).

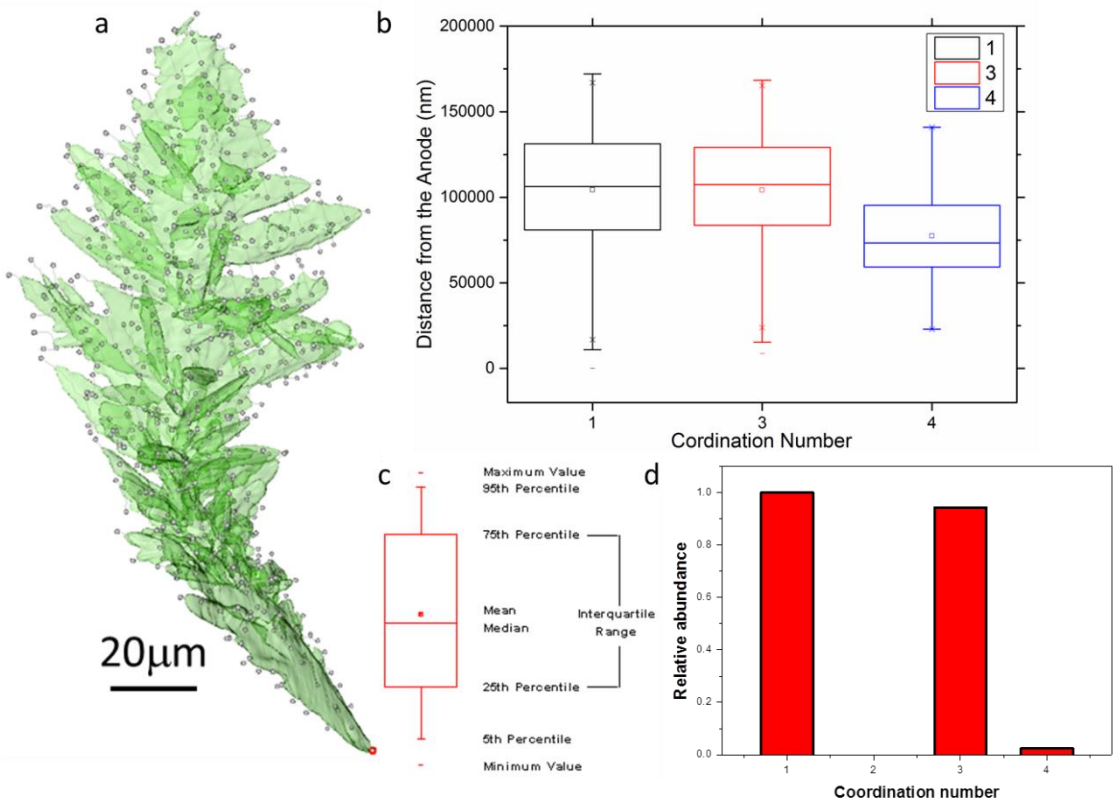


Figure 9 (a) A visualisation of skeletonised dendrite carried out using AVIZO software combined with shaded 3D image of the single dendrite (b) Scatter chart of the number of neighbours as a function of distance from the anode (c) description of the whisker plot[16] and (d) Histogram of coordination number. This approach also can be found in [17].

The coordination number of each node, and number of connections to neighbouring nodes, quantifies network connectivity (represented by the whisker box chart) suggests that this is a valuable approach to quantify the nature of this dendrite structure, offering a point of reference for other dendrite structures. The nodes with coordination number 1 represent the end tips and are the most abundant while those with coordination number 3 are the dendrite branches. There is no coordination number 2 as expected since it represents a line, and those with coordination number 4 occur at the lower part of the dendrite and in small quantity. For the first portion from the base of the dendrite, up to c.a. 50 µm, there are fewer neighbours hence almost no branches occur at that area as can be seen (Figurea). High coordination numbers indicate dense and branched dendritic structures while a low

coordination number demonstrates a relatively less dense and less branched dendritic structure. This observation can reflect and give a better insight on the growth mechanism. As seen the lower middle part of the dendrite (ca. 60 μm in height) is relatively thin, and yet there is high coordination number. This observation can be explained, as discussed in the first section of this chapter, by current density and by the counter electrode position and distance from the Zn dendrites. Therefore, it is expected that under these conditions the upper region of the dendrite will preferentially grow, resulting in a more developed branched structure and a higher coordination number than the lower and middle regions of the dendrite.

Identification of Mechanical Failure Sites in Electrochemical Dendrites

A new approach for mechanical testing was used for the first time to measure the mechanical properties of electrochemically deposited dendrites. (Figure 10)

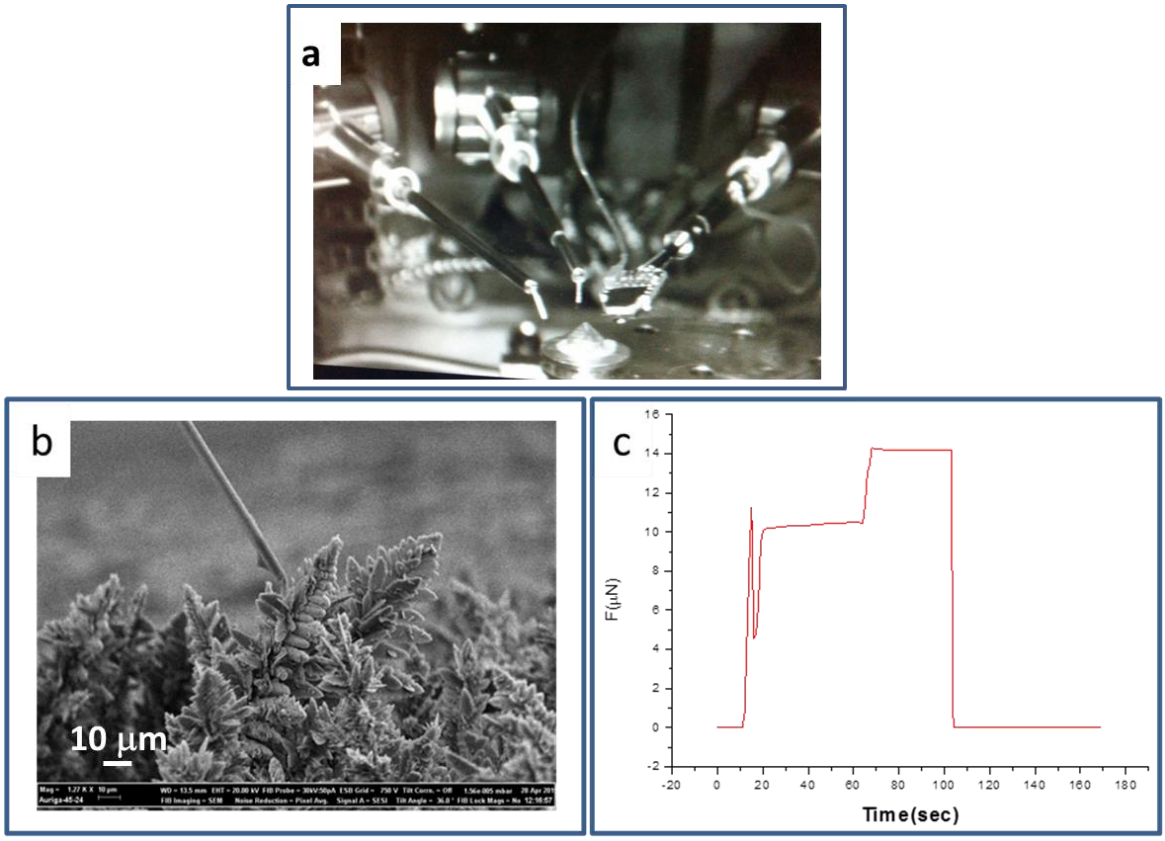


Figure 10 micromanipulator and force measurement analysis of a single dendrite. (a) The force measurement probes inside the Auriga 40 (b) SEM image of the micromanipulator pushing the dendrite (c) a graph showing the force applied to the dendrite until it fails.

For insight into the strength of these dendrites, a force measurement probe of Kleindiek Nanotechnik, (Reutlingen, Germany) was used for the first time for this purpose. This is a compact force readout tool for the micromanipulator which allows force measurements to be performed inside the SEM chamber on specific dendrites (Figure 10a). The force measurements are based on Hooke's law which states that the restoring force *F* of a spring is directly proportional to the spring displacement Δx, where *k* is the spring constant:

$$\Delta \mathbf{F} = \mathbf{k} \times \Delta \mathbf{x}$$

From the plot shown in (Figure 10c), the corresponding force applied to fracture the dendrite is 14 μN. We can see from the SEM image (Figure 10b) that other dendrites are

also affected when the target one is pushed. This means that in the 'forest' of dendrites it is difficult to accurately measure the fracture force of a single dendrite without taking into account other dendrites surrounding it, but it can be seen that the dendrite was broken at the bottom at the connection point to the electrode, an observation later supported by modelling. This suggests that this observation is still relevant for the individual dendrite since it confirms the point of failure. Further treatment will be needed to isolate a single dendrite for the extraction of a more accurate fracture force. A short video which describes the observation in Figure 10b and Figure 10c was recorded.

For a mechanical ABAQUS model (described before in the experimental section); a single dendrite was considered to comprise polycrystalline zinc with a Poisson's ratio of 0.26 and an Elastic Modulus of 97 GPa [12], with the assumption that the polycrystalline zinc is isotropic, linear and elastic. A maximum principal stress criterion was considered in this study to identify the critical stress, and hence, the critical force required to fracture this particular single dendrite.

A boundary condition was applied to the model by fixing the base (i.e. no displacement or rotation in any direction were allowed). Then a point force parallel to the base plane was applied at one of the branches near the top of the dendrite (Figure a) to mimic the experimental bending process of the single dendrite using the micromanipulator. The modelling results shown in Figure clearly indicate that the stress sits at the neck connecting to the base, as expected. Therefore the maxima reached in this case are just above the fracture strength, and the corresponding force is approximately 0.7 μN. [12]

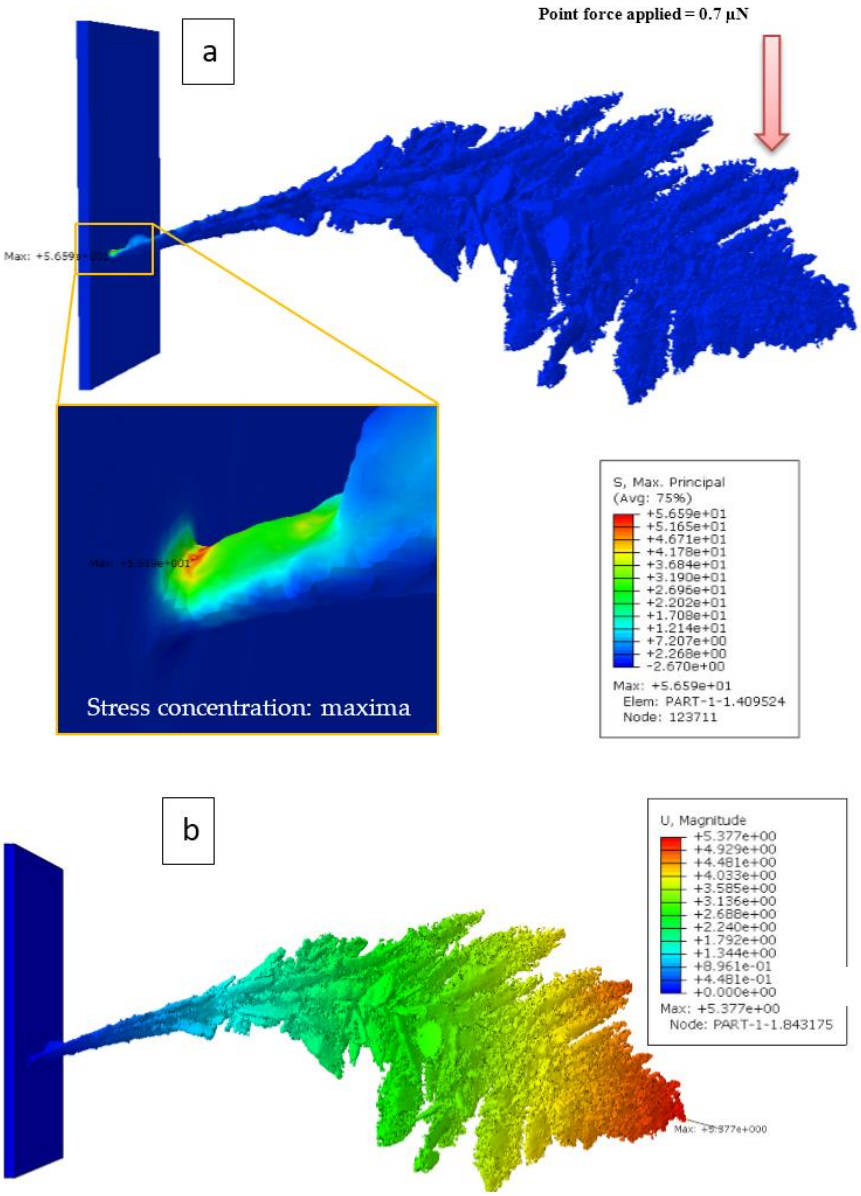


Figure 11 (a) maximum principal stress (unit=100MPa), the maximum stress at the neck = 566 MPa, which is just above the fracture strength (500 MPa). (b) Displacement (unit=0.1µm), the maximum displacement is 0.538 µm at the top of the dendrite.

The predicted force needed to break a single dendrite from the neck according the model is approximately 0.7 µN, which is much smaller than the force shown in the experiment using the micromanipulator (14 µN). The major reason for this difference is that the single dendrite presented in Figure 10b is not completely isolated as assumed in the model and it is supported by other dendrites; hence a greater force is needed to reach failure. Another

reason could be that the modelled dendrite could not be exactly the same one that was selected to perform the bending experiment, in terms of size and geometry.

According to the results, only a small force is required to break the dendrites. It gives additional insight into the degradation mechanism. Furthermore, the presence of a membrane could result in pressure on the dendrite base, especially when the dendrites are big and the membrane is dense. This could result in the detachment of dendrites, with a resulting capacity loss of active material [18].

In summary, integrating multi-length scale high resolution 3D imaging and modelling in the characterisation and identification of mechanical failure sites in electrochemical dendrites was successfully developed. A novel approach was used to enable the mechanical stabilization of a single dendrite. When combined with FIB-SEM tomography this allows high resolution 3D imaging of a full size dendrite. A combined experimental and modelling approach based on 3D imaging has been used to investigate zinc dendrite growth in a zinc-air battery. This approach is not limited to the Zn-air system but also it can be applied to other metal-air systems, such as Al-air, Mg-air and Li-air. However, Li-air cells would require a dry or inert atmosphere because of moisture sensitivity of lithium metal [19]. From the results it has been shown that the electrochemical dendrite morphology is more developed in the top region of the dendrite, further from the electrode, where there are long secondary arms. Micro-mechanical measurements were successfully introduced for the first time to study dendrites with a good agreement with the finite element simulations which suggest that dendrite necks connecting to the base are most likely the points of failure, as observed using the micro-mechanical manipulator.

4. Conclusions

Novel methods were developed and applied for the first time to provide high resolution 3D images of a single dendrite combined with modelling, and experiments using a micro manipulator identified that the dendrite's mechanical failure occurs at the bottom of the dendrites. We acknowledge the EPSRC (EP/L019469/1) for support. MB would like to thank the Alan Howard scholarship for further financial support (609201). We would also like to thank the MARS-EV project (FP7-2013-GC-Materials). The authors acknowledge the assistance of Dr David Eastwood and Prof Peter Lee from the University of Manchester (UK) for running X-ray experiments and access to v|tome|x CT machine.

5. References

[1] Müller S, Holzer F, Haas O. Journal of applied electrochemistry 1998;28:895.
[2] Scrosati B, Garche J. Journal of Power Sources 2010;195:2419.
[3] Harry KJ, Hallinan DT, Parkinson DY, MacDowell AA, Balsara NP. Nature materials 2013.
[4] Tariq F, Yufit V, Kishimoto M, Shearing PR, Menkin S, Golodnitsky D, Gelb J, Peled E, Brandon NP. J. Power Sources 2014;248:1014.
[5] Cooper S, Eastwood D, Gelb J, Damblanc G, Brett D, Bradley R, Withers P, Lee P, Marquis A, Brandon N. Journal of Power Sources 2013.
[6] Ender M, Joos J, Carraro T, Ivers-Tiffée E. Journal of The Electrochemical Society 2012;159:A972.
[7] Uchic MD, Holzer L, Inkson BJ, Principe EL, Munroe P. MRS bulletin 2007;32:408.
[8] Shearing P, Brett D, Brandon N. International Materials Reviews 201.55:347;0
[9] Shearing P, Brandon N, Gelb J, Bradley R, Withers P, Marquis A, Cooper S, Harris S. Journal of The Electrochemical Society 2012;159:A1023.
[10] Orso S, Wegst UG, Arzt E. Journal of materials science 2006;41:5122.
[11] Orso S, Wegst UG, Eberl C, Arzt E. Advanced Materials 2006;18:874.
[12] Ledbetter H. J. Phys. Chem. Ref. Data 1977;6:1181.
[13] Lee JS, Tai Kim S, Cao R, Choi NS, Liu M, Lee KT, Cho J. Advanced Energy Materials 2011;1:34.
[14] Farid Tariq, Peter Lee, Vlad Yufit, Billy Wu, Moshiel Biton, Nigel Brandon Zn-air results presentation. 2014.
[15] Tukey JW. 1977.
[16] Luntz AC, McCloskey BD. Chem Rev 2014;114:11721.
[17] Zhu W, Gaetani GA, Fusseis F, Montési LG, De Carlo F. Science 2011;332:88.
[18] Owen JR. Chem. Soc. Rev. 1997;2.6:259
[19] Cho M, Trottier J, Gagnon C, Hovington P, Clément D, Vijh A, Kim C-S, Guerfi A, Black R, Nazar L. Journal of Power Sources 2014;268:565.
[20]

Yufit, V., Tariq, F., Wu, B., Biton, M., Merla, Y., Eastwood, D. and Brandon, N. P. "In-Operando X-ray Tomography Studies of Dendrite Formation in Zinc-Air Batteries." Meeting Abstracts. No. 4. The Electrochemical Society, 2014.